SEVENTH EUROPEAN ROTORCRAFT AND POWERED LIFT AIRCRAFT FORUM

Paper No. 31

WIND TUNNEL INVESTIGATION OF HIGH SPEED ROTOR NOISE

H. Tadghighi and I.C. Cheeseman

University of Southampton
Southampton, U.K.

September 8 - 11, 1981

Garmisch-Partenkirchen
Federal Republic of Germany

Deutsche Gesellschaft für Luft- und Raumfahrte e. V.
Goethestr. 10, D-5000 Köln 51, F.R.G.

WIND TUNNEL INVESTIGATION OF HIGH SPEED ROTOR NOISE

H. Tadghighi and I.C. Cheeseman

University of Southampton
Southampton, U.K.

SUMMARY

The ability to model a helicopter rotor in forward flight aeroacoustically and to make reliable noise measurements represents a research objective which, if achieved, has important cost and design implications for the helicopter industry.

A high speed model rotor (tip Mach Number of 0.75) has therefore been developed at Southampton University to investigate tail rotor noise in forward flight conditions. The existing 2.1 x 1.5m low speed (30m/sec) closed circuit wind tunnel has been modified and utilised to enable acoustic measurements of forward flight to be made. Check tests at the Royal Aircraft Establishment Farnborough in the 24ft anechoic wind tunnel have shown excellent agreement with the Southampton tests.

The model rotor noise data is found to correlate well with full scale helicopter rotor values. Simultaneously recorded aerodynamic performance of the model rotor (blade loading, steady thrust, torque and trimmed moments) has been compared with theoretical aeroacoustic treatments. This report discusses the selected theoretical models (Wright, Lowson and Ollerhead, Davidson & Hargest and Hawkings) and compares this prediction with the experimental results.

Finally this report concludes that the model rotor accurately simulates full scale rotor aeroacoustic data.

NOTATION

a_o speed of sound m/sec

b blade span (m)

B number of blades

c blade chord (m)

C_{L_T} overall rotor lift coefficient, $L/\frac{1}{2}\rho_o V_T^2 S$

C_{L_λ} harmonic lift coefficient

f frequency (Hz)

F_T total torque force on rotor ($LT\sin\beta$)

k observation factor (dB)

K power law factor

K_x, K_y normalised wave number, $\pi fc/U$ and $mb/2$ respectively

L_o mean steady blade loading (N)

L_s harmonic loadings (N)

m sound harmonic number

M_e effective Mach number (0.85k)

N rotor shaft frequency (Hz)

q mode numbers ($mB \pm s$)

r rotor radius (m)

R observer distance from rotor centre

S blade plan area (m^2)

s loading harmonic number

SP sound pressure N/m^2

S_t Strouhal Number

T total thrust (N)

U mean flow velocity (x-direction)

u,v,w perturbation velocity m/sec

V_T rotor tip speed m/sec

α_s blade loading harmonic coefficient $\alpha_s = L_s/L_o$

β force (or effective blade lift) angle

σ observer elevation angle to rotor disc

ρ_o air density Kg/m^3

1. *INTRODUCTION*

For civilian operations, high levels of noise from helicopters or V/STOL aircraft restrict their use for city centre transportation. In military use high noise levels give early warning of approach to an enemy. Clearly, there is a need to control the noise levels generated with a minimum performance penalty.

In the present state-of-the-art, the external noise of the helicopter is not predicted accurately for most flight conditions. The reason is that helicopter external noise is generated by several sources such as the main rotor noise and tail rotors and the engine. The noise arises from aerodynamic

excitation which may be considered to be the ideal noise arising when the system is operating in isolation in clean flow flux, the secondary but not necessarily the less important terms due to interaction effects and real flow conditions.

The difficulty of finding the basic noise of a near ideal rotor operating in clean flow without pilot control inputs is only possible in a controlled environment like an aeroacoustic wind tunnel. Carefully controlled undisturbed perturbations in the flow may then be introduced and the effect measured and compared with theoretical prediction.

In this paper a wind tunnel test of a high tip speed helicopter is discussed in near ideal flow as well as the effect of testing in another tunnel with different flow conditions. Various theoretical methods were examined in relation to the measured noise and aerodynamic performance of the rotor.

2. MODEL ROTOR RIG

2.1 The 1.27m Diameter Helicopter Rotor

This model rotor (Fig.1) was designed to allow tests to be made at rotor tip speeds equal to those currently in full scale use. The diameter (1.27m) was restricted by the need to mount the rotor with acceptable aerodynamic interference levels in the closed test section of the University 2.1m x 1.5m (7ft x 5ft) tunnel, while the blade span (0.57m) was then defined by minimum size of the hub. The blade chord (60.3mm) was fixed because carbon fibre spar blades were needed to accept centrifugal loads and an existing mould could be borrowed from the Royal Aircraft Establishment, Structures Department. The result was a rectangular planform of aspect ratio 8 for the blade, conveniently midway between that used for current tail rotor and main rotor design.

The rotor blades have only a feathering freedom. The blade pitch can be changed remotely in the collection and cyclic sense through a swashplate; position sensors are fitted. The blades are made of carbon fibre spars with the surrounding shape in polyurethane moulded to the NACA 0015 contour. The present rotor head design allows two or four blades to be fitted. Strain gauge balances, situated immediately below the rotor head, are capable of giving rotor thrust, side force, H-force (drag), rolling moment and pitching moment (Fig.2).

The rotor is driven by a 26 KW variable speed electric motor. The torque used by the rotor is measured by a foil torque rosette located on the drive shaft. The strain gauge output varies linearly with applied load as shown in Fig.3.

3. INSTRUMENTATION

3.1 Blade Strain Gauges

One 'Master' blade is fitted with four pairs of strain gauges (semi-conductor type 120p) distributed along its span, and the remaining 'slave' blades are fitted near their roots with one pair each. The disposition of gauge pairs is shown in Fig.4, each pair is given a double digit notation,

the first digit being the number of the blade to which it is fitted, the second digit signifying the location of the pair on that spar; each gauge of a pair is also sub-scripted U or L surface. Thus we have gauges 14U and 14L at the tip of the Master on the upper and lower surfaces respectively, and 41U and 41L at the inboard end of blade No.4 likewise.

The object of these strain gauges is to measure flapwise loading moments and hence to obtain an indication of lift distribution. Each pair of gauges is fitted into a strain gauge bridge so doubling the sensitivity of the system. The output from each gauge pair is taken out through a twenty-channel slip-ring assembly.

3.2 Calibration

3.2.1 Lift

Vertical loads were applied simply, as shown in Fig.5a. The strain guage output readings, provided by a 'Boulton-Paul Transducer Meter' are plotted against applied load in Fig.6; a consistent linear output without hytersis is found.

3.2.2 Horizontal forces

Loads were applied at a blade-root fitting, as shown in Fig.5b. The results for both longitudinal and lateral application of forces are plotted in Fig.7, where the symmetry of the system and the sensitivity are seen to be good. No cross-coupling (i.e. longitudinal due to lateral force) is found. Because the balance is some distance below the rotor head, appearance of a side-force gives rise to an apparent moment, as shown in Fig.8.

3.2.3 Moments

To produce a series of nose-up pitching moments, a beam was attached to the head-loading device, as shown in Fig.5c, for moment calibrations, this beam was turned 90^{o}. The plot of the moment output signals is shown in Fig.8. Since no sideways force is produced by the application of pure moments, it is possible to resolve a measured moment and sideways force into head moment and force using these curves.

4. ROTOR AERODYNAMIC PERFORMANCE

The rotor performance was investigated by measuring the thrust T from the lift balance and the power P by means of the wire gauge torque rosette on the shaft. The rotor pitching and rolling moments were reduced to zero by application of the cyclic pitch control. Fig.9 shows a plot of the rotor power coefficient C_P ($\equiv P/\frac{1}{2}\rho S V^3_{tip}$) against $C_T^{3/2}$ ($\equiv T/\frac{1}{2}\rho V^2_{tip}$) for all test conditions. As expected this power coefficient at constant thrust for wind speeds of 15m/sec and 30m/sec is lower for a trimmed rotor than for a near hover condition.

5. NOISE EXPERIMENTS

5.1 The Acoustic Wind Tunnel

This facility has been described elsewhere in detail (Ref.1) so only brief relevant data are given here.

Acoustic treatment has been applied to the flow-circuit of the existing low speed wind tunnel in order to restrict the noise generated by the fan reaching the 2.13 x 1.52m working section. The walls of the working section have also been treated acoustically to reduce the reflection of acoustic energy from model generated noise. The maximum wind speed in this working section with the tunnel acoustic treatment in place is about 30m/sec.

5.2 Acoustic Instrumentation

All measurements referred to in this paper have been made with half inch microphones (B&K 4133) fitted with nose-cones (B&K 2619) aligned with the free stream. Ref.1 shows that the nose cones are satisfactory for noise measurement in the tunnel. A streamlined vertical support was mounted in the tunnel and the microphones were then cantilevered out forwards and sideways. The microphones were located at a radial distance of 2.8 directly upstream from the rotor centre, as measured along directions 5^{o} and 15^{o} down from the horizontal plane through the centre of the rotor (Fig.10). Ref.1 has shown that the streamlined support does not produce any noise contamination of the test noise results.

The microphones were connected through cathode followers (B&K 2619) to frequency analysers (B&K type 2120) and a level recorder for on-line inspection, and to a twin channel recorder (Revox 700A) for subsequent examination in the Data Analysis Centre or elsewhere (Fig.11).

5.3 Range of Experiments

Noise was recorded at two microphone positions, the measured data then being used for spectral analysis (1% band-width and third-octave), as a basis for investigations into the nature of rotor noise, and for correlation with aerodynamic loading information. From the rotor rig balance, total thrust, side forces and moments have been recorded. The moment channel information was used to adjust the cyclic pitch controls to produce a trimmed (zero moment) rotor state. The outputs of the blade strain gauges measuring flapwise bending were recorded to study harmonic blade loadings which are related to rotational noise (Section 8). All these measurements were taken for ranges of rotor speeds (2400, 2600, 2800, 3100 rpm) and collective pitch angles, at tunnel speeds of 15m/sec and 30m/sec. Operating the rotor in the tunnel with no airflow was not possible because of intense recirculation effects so a very low forward speed of 1.5m/sec was used to approximate to the hover case.

5.4 Background Noise

Experiments were made with tunnel wind speeds of 15 and 30m/s. In addition to simulate hover measurements tests were made with a wind speed of 1.5m/sec to minimise recirculation effects. There was concern that the tunnel background noise and/or the noise of the electric drive motor and transmission would interfere with measurements in the acoustic working section. Figure 12 shows a 1% spectrum for the rotor rig running without rotor blades and with no wind tunnel airflow, for the complete rotor rig installed in the tunnel but non rotating and the tunnel operating at 30m/s and finally the rotor turning at 2800 RPM (tip speed 202m/s) with 4^{o} collective pitch applied and with a forward airspeed of 30m/sec. The rotor is trimmed using the cyclic pitch controls to produce zero rolling and pitching moments. The figure shows that even at the worst condition (about 800 Hz) the rotor noise exceeds the sum of the rotor and background noise thus indicating that genuine rotor blade noise was being recorded.

5.5 Comparison of OASPL Results with Full Scale Prediction Methods

Since the microphones are only situated 1.7 rotor diameters upstream of the centre of the rotor there was some doubt that they were in the far field. It was therefore decided to check the overall noise levels with the simple but well tried formula of Davidson and Hargest. This formula relates the OASPL at 500 feet (150m) to the tip speed V_T, the overall rotor lift coefficient C_{L_T} = Rotor Lift/$\frac{1}{2}\rho V_T^2 S$, the blade plan area S and an observation factor k which includes a directivity and a forward speed term

$$(OASPL)_{500} = 60 \log V_T + 20 \log C_{L_T} + 10 \log S + k \qquad (1)$$

The result was corrected to 2.4m by inverse square law. The results for a range of tests are shown in Figure 13 where the experimental values are plotted against the values estimated from equation (1) using measured values of V_T and rotor thrust. Bearing in mind the extrapolation of rotor scale and distance the agreement is most encouraging. It is noted that the calculated values of noise exceed the experimental values for the higher collective pitch values and therefore the higher lift values. The Davidson and Hargest model assumes a thrust dipole for its directivity model whereas noise at low thrust values will be torque dominated and hence an underestimate of the noise was expected and found. However their formula is based on real helicopter noise which included maldistribution noise due, for example, to fuselage interference and hence there was likely to be an element of excess noise over that of the model rotor running in near ideal flow without pilot control inputs and with very stiff blades which minimised any aeroelastic loads. The overall agreement is therefore considered satisfactory.

5.6 General Spectral Characteristics

For the near hover condition a 1% bandwidth spectrum of the rotor noise at 4° collective pitch and 2800 RPM in Figure 14 is shown. The rotational noise spectrum stands out clearly - the first 16 harmonics of the blade passing frequency (1f) are easily identified. The corresponding spectrum at the same rotational speed and a tunnel speed of 30m/sec is also shown. The changes in the spectrum show first that certain rotational harmonic levels have altered due to the change in the loading pattern and second that the broadband noise level has increased by about 4 dB. On a V^6 law based on the advancing blade tip speed this increase should be about 3.6 dB.

6. LOW FREQUENCY BROADBAND NOISE

6.1 Spectrum Characteristic

The apparent low frequency "broadband noise" region is often a combination of broadband noise and the higher harmonic rotational (discrete frequency) noise. It is necessary to select a filter bandwidth which detects these harmonics and so gives an accurate measure of the broadband energy. It was found that a third-octave bandwidth filter was most suitable.

Typical third-octave bandwidth analysis results are presented in Fig.15. It has been suggested by Leverton (2) that 8 dB "fall-off" either side of "peak" is a typical value for a real helicopter (i.e. this could be applied

from $f_H/2$ to 4 f_H (where f_H is the peak frequency). The fall-off rate within the frequency range mentioned above was found to be 8 dB for the model rotor.

6.2 Variation with Thrust

Fig.16 plots the variation in peak SPL of the broadband noise with the thrust of the model rotor, showing that the noise exhibits trends which vary with forward speed. The peak SPL varies at T^4 at 15m/sec airspeed as T^3 for 30m/sec and as T^2 for near hover. The last relationship agrees with Leverton's[2] analysis for a real helicopter in hover.

6.3 Variation with Thrust of the Advancing Blade in Forward Flight

The noise received upstream may be dominated by that produced by the advancing blade so peak SPL of the broadband noise has been plotted against advancing blade thrust deduced from the blade gauge value and $\psi = 90^o$. The results are plotted for the forward speeds in Fig.16 which shows better collapse and indicates that peak SPL varies $(T_{\text{advancing blade}})^2$, a result which must agree with that found in near hover for the whole rotor.

6.4 Frequency Characteristic

The low frequency broadband noise "peak" is normally associated with Strouhal number relationship

$$f_H = S_t \, V_{\text{advancing}}/c \qquad (2)$$

where f_H = 'Hump' frequency

$V_{\text{advancing}}$ = rotor advancing blade tip speed

c = chord

From Fig.15 the Strouhal number takes the values 0.75, 0.78 and 0.8 for near hover, 15m/sec and 30m/sec respectively; the value S_t = 0.8 was found by Leverton (2) for real helicopter.

7. HIGH FREQUENCY BROADBAND NOISE

7.1 Spectrum Characteristics

Fig.17 shows a 1% bandwidth analysis of the various test cases for the range of 2000 < FREQ < 20000. It indicates that there is also a "hump" in 'high frequency' broadband noise at a frequency of about 12 KHz approximately, but the hump is not well defined. It was found by Leverton (2) analysis that the high frequency "hump" for a model rotor to be around ≈12KHz.

8. THEORETICAL PREDICTIONS

8.1 The Theoretical Investigation into the Aeroacoustics of a Rotor

The general formulae for prediction of rotational noise by S.E. Wright (3) is given by

$$SP_{mB} = \sum_{s=a}^{s=b} \frac{\alpha_s}{2} \left| \{K_T - K_F \frac{q^-}{mB}\}\gamma_{q^-} - \{K_T - K_F \frac{q^+}{mB}\}\gamma_{q^+} \right| \qquad (3)$$

where

$\gamma_q = mB\, J_q\, (mB\, M_e \cos\sigma)$ (directivity function of q^{th} mode)

$\alpha_s = {}^{L_s}/_{L_o}$ (harmonic blade loading coefficients)

$q = mB \pm s$ (mode number)

$K_T = {}^{N}/_{R_{ao}}\, T_r \sin\sigma$ (thrust constant)

$K_F = {}^{N}/_{R_{ao}}\, {}^{F_T}/_{M_e}$ (torque force constant)

S = harmonic number

The $|\alpha_s|$ values in equation (3) will contribute to the rotational noise level significantly. Therefore an accurate evaluation of $|\alpha_s|$ is necessary to improve the theoretical noise models. Hence a set of simultaneous equations are developed based on S.E. Wright (3) method for the calculation of $|\alpha_s|$ by employing $|SP_{mB}|$ (second pressure for each harmonic) from the experimental noise spectrum.

The matrix formation of the first harmonic (m = 1) for a given $M_e \cos\sigma = 0.5$ and B = 4 is determined by

$$\gamma_{q \to 0} \qquad {}^{S}/_{(1 - M_e \cos\sigma)} > mB > {}^{S}/_{(1 + M_e \cos\sigma)} \qquad (4)$$

(upper cut off) (lower cut off)

which consists of terms for which $2 < S < 6$ plus the contribution from the Gutin (4) (steady load) model which gives

$$\begin{vmatrix} \text{Gutin Steady Load Term} \\ SP_{s=0} \\ SP_{s=3} \\ SP_{s=4} \\ SP_{s=5} \end{vmatrix} = \begin{vmatrix} \gamma_{q_4}\ \alpha_o & \gamma_{q_4}\ \alpha_o \\ (\gamma_{q_7} + \gamma_{q_1})^{\alpha_3/2} & \alpha_3/_8(\gamma_{q_1} + 7\gamma_{q_7}) \\ (\gamma_{q_o} + \gamma_{q_8})^{\alpha_4/2} & \gamma_{q_8}\ \alpha_4 \\ (\gamma_{q-1} + \gamma_{q_9})^{\alpha_5/2} & \alpha_5/_8(9\gamma_{q_9} - \gamma_{q-1}) \end{vmatrix} \begin{vmatrix} K_T \\ -K_F \end{vmatrix} \qquad (5)$$

where SP_s = sound pressure fluctuation of mB_s mode.

Equation (5) was solved using the acoustic noise measured to obtain the values of α_s. In order to solve the equation (5) in this way, a relationship between SP_{mB} (i.e. total sound pressure for each harmonic) and SP_{mBs} (i.e. sound pressure due to individual harmonic blade loadings) must be found. The general equation for the sound pressure in terms of sound pressure due to blade loading harmonic is given by

$$SP_{mB} = \sum_{s=0}^{\infty} SP_{mBs} \tag{6}$$

where the range of values of s is found from equation (4) for each sound harmonic. The expansion of equation (6) in terms of α_s for the first, second, third and fourth harmonic given $M_e \cos\sigma$ (i.e. $M_e \cos\sigma = 0.5$), B = 4 and microphone position 5° and 15° below plane of the rotor are given by:

Microphone 5°

$$SP_{mB=4} = C_o\alpha_o + C_3\alpha_3 + C_4\alpha_4 + C_5\alpha_5$$

$$SP_{mB=8} = C_5\alpha_5 + C_6\alpha_6 + C_7\alpha_7 + C_8\alpha_8 + C_9\alpha_9 + C_{10}\alpha_{10} + E_1$$

$$SP_{mB=12} = C_7\alpha_7 + C_8\alpha_8 + C_9\alpha_9 + C_{10}\alpha_{10} + E_2 \tag{7}$$

$$SP_{mB=16} = C_9\alpha_9 + C_{10}\alpha_{10} + E_3$$

where $C_q = \gamma_q \pm (K_T - K_F)$

$E = \sum_{i=11}^{n} C_i \alpha_i$ (which is found to be extremely small).

Microphone 15°

$$SP_{mB=4} = A_o\alpha_o + A_3\alpha_3 + A_4\alpha_4 + A_5\alpha_5 + A_6\alpha_6$$

$$SP_{mB=8} = A_5\alpha_5 + A_6\alpha_6 + A_7\alpha_7 + A_8\alpha_8 + A_9\alpha_9 + A_{10}\alpha_{10} + F_1 \tag{8}$$

$$SP_{mB=12} = A_7\alpha_7 + A_8\alpha_8 + A_9\alpha_9 + A_{10}\alpha_{10} + F_2$$

$$SP_{mB=16} = A_9\alpha_9 + A_{10}\alpha_{10} + F_3$$

where $A_q = G_q \pm (Q_T - Q_F)$

$$F = \sum_{i=11}^{n} A_i \alpha_i$$ which is found to be very small.

When the values of α_s ($s = a, b$) from equations (7) and (8) were found, then the experimental results were compared with these theoretical values. Fig.18 is presented for a radial position of (0.85R). (The agreements are encouraging). This is a sample of many results which have been obtained for a wide variety of rotor conditions and for distributed turbulence and simulated gust and rotor gust and rotor vortex passage effects. In addition radiation noise offers an opportunity to obtain information on rotor blade harmonic loadings.

9. DETERMINATION OF HARMONIC LOADING FACTOR DERIVED FROM THE LOWSON AND OLLERHEAD MODEL

The general equation for prediction of rotational noise by Lowson and Ollerhead (5) is given by

$$SP_{mB} = \sum_{s=a}^{s=b} S^{-K} \left| K_T \gamma_{q^-} - K_F \frac{q^-}{mB} \gamma_{q^-} + K_c \cos\sigma \gamma_{q^-} \right| \qquad (9)$$

where K_c = radial force function (which is normally not important for a rotor).

The equation (9) was rearranged to calculate the values of $|K|$ (power law factor), which is theoretically modelled for the harmonic loadings of a rotor by Lowson and Ollerhead (5) as

$$S^{-K} = {}^{L_S}/_{L_o} = |\alpha_s| \qquad (10)$$

where L_s = harmonic loadings (N)

L_o = mean steady blade loadings (N)

S = loading harmonic number

K = power law factor.

Therefore the equation for the n^{th} harmonic is given as

$$\sum_{i=m_1}^{m_2} S_i^K = {}^1/_{|SP_n|_{exp}} \left| K_T - K_F^{q^-} \right| / n \left| j_{q^-} (n M_e \cos\sigma) \right| \qquad (11)$$

where $|SP_n|_{exp}$ = experimental sound pressure values.

Fig.19 shows a plot of K values obtained from equation (11) against skew angles (i.e. $^{V_i}/_{V_t}$ is skew angle, representing the rotor aerodynamic performance) for a variety of the rotor test runs. The results indicate that due to non-scattering of the K values there is no unexpected change in the tunnel flow (i.e. no circulation and/or separation in the working section of the wind tunnel) to contaminate the noise signal received by the microphones. In addition, for a value of K = 2.4 the rotational noise values of the rotor can be predicted within $\pm$ 0.5 dB. It is encouraging that K = 2.4 is comparable with Lowson and Ollerhead's (5) K values of 2.5 which is based on a real helicopter harmonic loading data.

10. THICKNESS NOISE OF THE MODEL ROTOR (D. HAWKINGS (6))

The thickness noise of the model rotor was calculated by employing Hawkings (6) theoretical thickness noise model. The model is based on the volume displacements of the flow (i.e. monopole), which could be significant for the high speed rotors (i.e. depending on the shape of the blades). Fig.20 shows the comparison of rotational noise harmonics (i.e. up to 10th) with thickness noise of the model rotor for two extreme speeds of the experiments (i.e. 2400 rpm, 3100 rpm). The levels of the thickness noise of the rotor is 10dB below the rotor noise levels. Therefore the thickness noise of the rotor does not have any significant effect on the rotor rotational noise levels up to the 10th harmonic (up to a tip speed of 250 m/sec and forward speed of 30 m/sec for 0015 wing section).

11. VARIATION OF ROTATIONAL NOISE HARMONIC AND AERODYNAMIC FORCES WITH TIME DURING A TEST RUN WITH CONSTANT OPERATING CONDITIONS

The behaviour of individual rotational noise levels with respect to harmonic loadings was investigated for a single test run. The two signals (i.e. noise and aerodynamic forces) have been acquired simultaneously for over 200 revolutions of the rotor disc.

Figs.21 and 22 show the corresponding power spectrum density of the noise and aerodynamic forces averaged over three consecutive rotor revolutions. These spectra illustrate a high degree of repeatability. The "mean" and "standard-deviation" values of these successive psDs signals were obtained for frequency bandwidth of 7Hz, and this is plotted in Figs.23 and 24. The PDF (Probability Density Function) of the rotor aeroacoustic (averaged over 3 revolutions) compared with the overall PDF (averaged over 50 revolutions) confirms the repeatability of the overall result.

The individual harmonic variation with time was next considered. The noise signals up to the tenth harmonic and the corresponding loading harmonics are shown in Figs.25 and 26. The way that the rotational noise values follow corresponding harmonic loading is clear up to the tenth harmonic. The higher rotational noise harmonics (above the 6th harmonic) show a large fluctuation in amplitude. This unsteadiness is due to the individual blade loading harmonic L_λ (λ = 1, 2.....n) as shown in Fig.27. This large variation in loading harmonics for a near ideal situation, i.e. no pilot inputs, aircraft motion, clean and steady flow and stiff rotor blades, underlines the difficulty of producing a detailed theoretical loading model to describe the time variation of these loads.

12. COMPARATIVE STUDIES OF THE ROTOR AEROACOUSTIC IN TWO DIFFERENT ACOUSTIC TUNNELS

The 1.27m model rotor has been tested in the Royal Aircraft Establishment 24ft acoustic tunnel in undisturbed flow conditions, Fig.28. The experimental procedure was identical to the one used at Southampton University (i.e. mic distance, advance ratio, collective pitch). Fig.29 shows the noise spectra from the model rotor obtained in these two tunnels. The results show that these two spectra only differ in the region of 1000 Hz < f < 3000 Hz. This discrepancy has been investigated by employing the method of Section 8.1 to predict the rotational noise level in this region, as shown in Fig.29. As a result it was concluded that the higher level of noise in this part of the spectrum is due to the rotor aerodynamic changes as shown in Fig.30. Hence it was suspected that the two tunnels had different turbulence spectra and that this might account for the measured noise in the range of 1000 < f < 3000 Hz.

The turbulence values of the RAE tunnel were calculated by employing a two-dimensional thin aerofoil theory in incompressible turbulence flow. Sears (7) considers the function of an upwash pattern of the form given by

$$W\, e^{i(2\pi ft - K_x x + K_y y)}$$

where $K_y = mb/2$ and $K_x = \pi fc/U$.

For this form of velocity distribution Mugridge (8) gives a relationship for three-dimensional unsteady lift on the airfoil as

$$L = \bar{\omega}\, \pi\, e\, \rho_o\, U \left| E_{Sears}{}^{*}\, E_{Mugridge} \right| \qquad (12)$$

where E_{Sears} = Sears' function $= \dfrac{1}{1 + 2\pi K_x}$

and $E_{Mugridge} = \dfrac{K_x{}^2 + {}^2/_{\pi^2}}{K_x{}^2 + K_y{}^2 + {}^2/_{\pi}}$

Therefore by integration and rearrangement of the equation (12) the turbulence intensity can be given by

$$\left| \frac{\overline{|W(K_x, K_y)|^2}}{U^2} \right|_{(intensity)^2} = \frac{\left| \overline{\Delta |CL(K_x, K_y)|^2} \right|_{mB(experimental)}}{4\, b^2 \pi^2\, E_1\, E_2\, E_3} \qquad (13)$$

where $E_1 = \dfrac{1}{1 + 2\pi\, K_x}$

$$E_2 = \frac{K_x{}^2 + {}^2/_{\pi^2}}{K_x{}^2 + {}^2/_{\pi^2} + K_y{}^2}$$

and $E_3 = \left(\frac{\sin(K_y)}{K_y}\right)^2$

Turbulence intensity of the RAE tunnel was calculated from equation (13) for

$$\overline{\Delta|CL(K_x, K_y)|^2}_{experimental} = \overline{|CL\ s|^2}_{RAE(exp)} - \overline{|CL\ s|^2}_{SU(exp)} \qquad (14)$$

where $\overline{|CL\ s|}$ = harmonic lift coefficient components contributed to each harmonic noise level (i.e. mB).

The results are shown in Fig.31 for frequency range of 1000 < freq < 3000, which indicates that the excess noise in this region (1000 < f < 3000) is due to the high turbulence intensity in the RAE tunnel flow. Also as it was found that the increase in turbulence intensity of free stream would in general tend to increase the high order harmonic loadings of a rotor.

13. CONCLUSIONS

The aeroacoustic results from a model rotor have been shown to correspond to full scale results.

The calculation of aerodynamic loads and rotational noise is good, so opening the way to predict aerodynamic loads from noise experiments.

Detailed studies into the real time analysis of a rotor aeroacoustic signal have been verified for a full correlation between a rotor noise value and the corresponding unsteady loadings. It has been shown that the 'thickness noise' values of the model rotor have no significant effects on the rotational noise results (up to 10th harmonic).

The acoustic tunnel was found to be a very satisfactory tool for making controlled noise experiments on model helicopter rotors provided that the flow in the working section is not contaminated by high turbulence intensity for 100 < f < 10000 Hz.

REFERENCES

1. I.C. Cheeseman, H. Tadghighi and B. Prichard — The Use of an Acoustic Wind Tunnel for Aeroacoustic Research. Jahrestagung der DGLR, Aachen, 12 May 1981.

2. J.W. Leverton — A Study of Helicopter Rotor Noise with Particular Reference to Transient Effects. Ph.D. Thesis, I.S.V.R., University of Southampton, 1977.

3. S.E. Wright — Sound Radiation from a Lifting Rotor Generated by Asymmetric Disc Loading. I.S.V.R., Southampton University, August 1968.

4. L. Gutin	On the Sound Field of a Rotating Propeller. NACA Tech Memo No.1195, Translation 1947.
5. M.V. Lowson and J.B. Ollerhead	Studies of Helicopter Rotor Noise. Lab Report No.W.R.62-9.
6. D.L. Hawkings and M.V. Lowson	Tone Noise of High Speed Rotors. Progress in Aeronautics and Astronautics, Volume 44, 1976.
7. W.R. Sears	Some Aspects of Non-Stationary Aerofoil Theory and its Applications. Journal of Aeronautical Sci., 8, pp.104-108, 1941.
8. B.D. Mugridge	Gust Loading on a Thin Aerofoil. Journal of Sound and Vibration 18, pp.301-310, August 1971.

ACKNOWLEDGEMENTS

Grateful acknowledgement is made to the Ministry of Defence (Procurement Executive) and the Royal Aircraft Establishment. Also to our many colleagues who contributed to the experimental work, in particular Professor J. Williams who has made valuable suggestions as the work has proceeded.

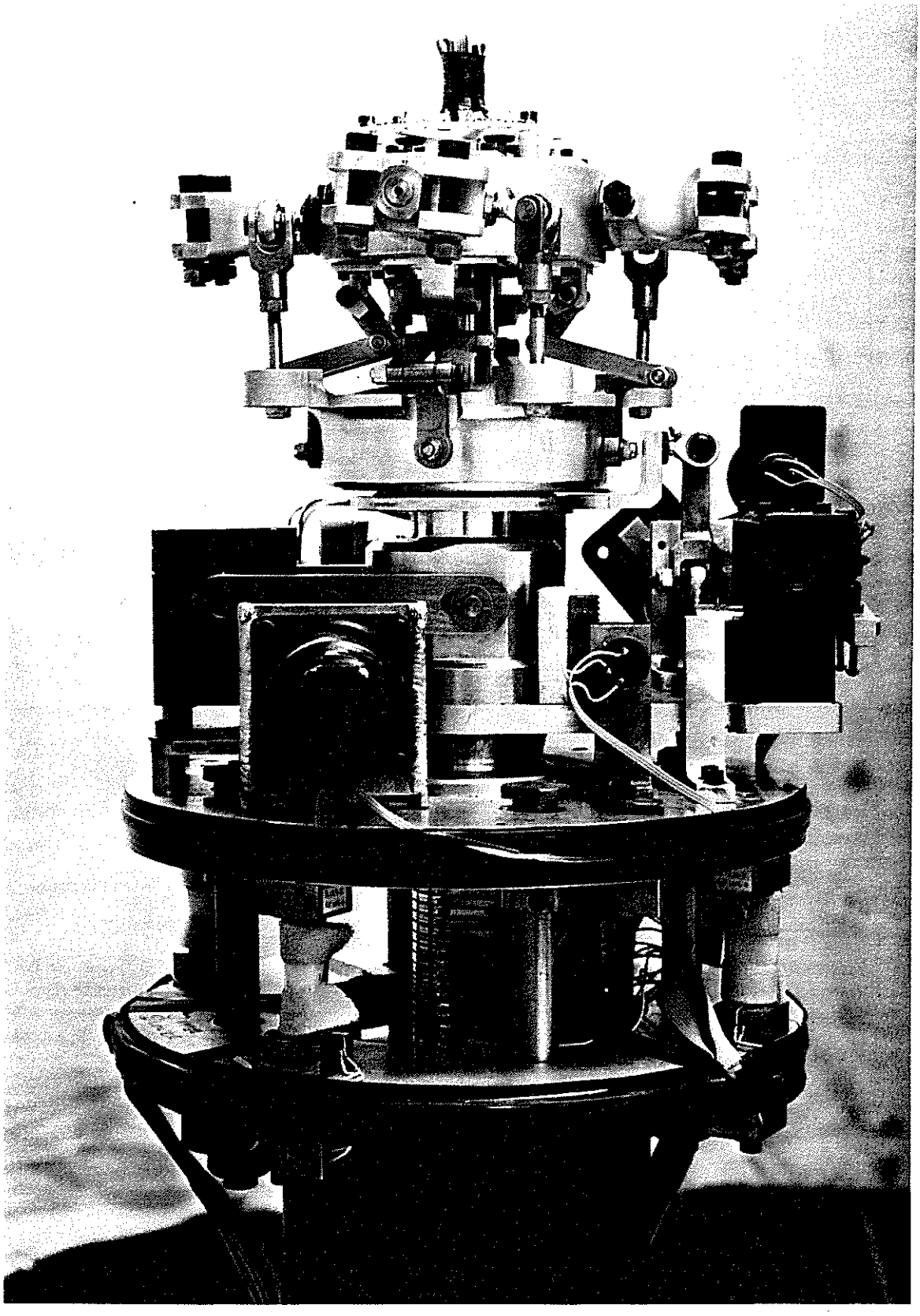

FIG.1 MODEL ROTOR HEAD

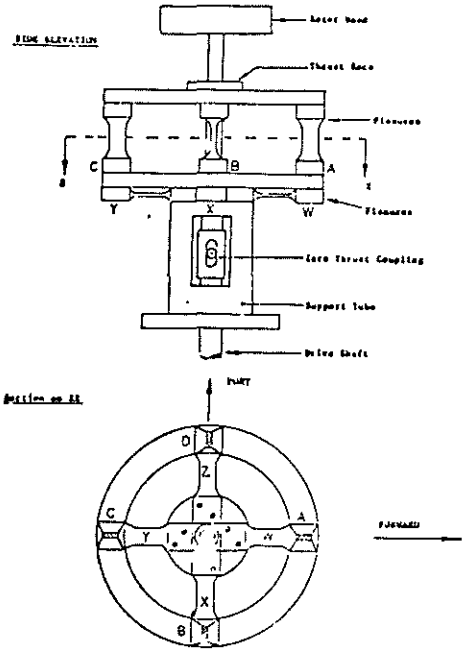

FIG.2 SCHEMATIC OF BALANCE ARRANGEMENT

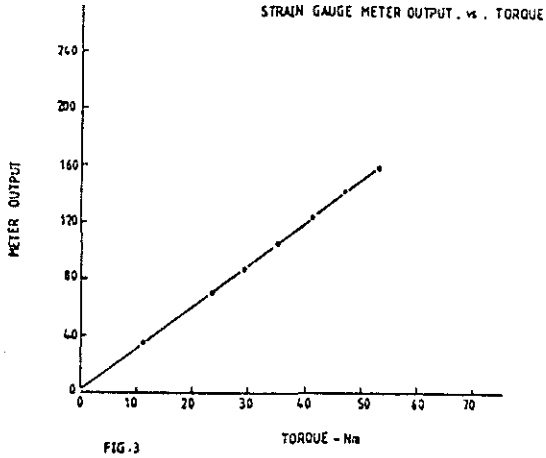

FIG.3

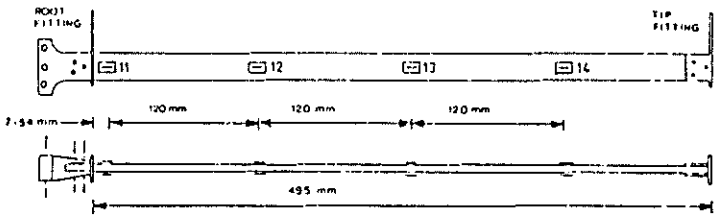

BLADE	MASTER (NO1)				SLAVES (NO 2,3,4)
GAUGE	11	12	13	14	21, 31, 41
RADIUS (mm)	142·5	262·5	382·5	502·5	142·5

FIG 4 MASTER BLADE SPAR - STRAIN GAUGE LAYOUT.

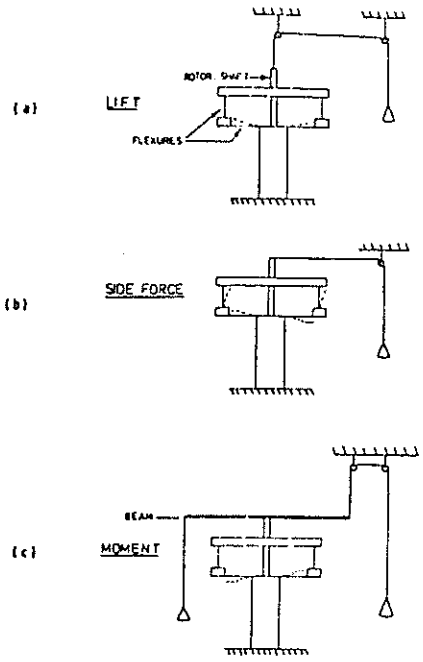

FIG 5 LOADING FLEXURES FOR CALIBRATIONS

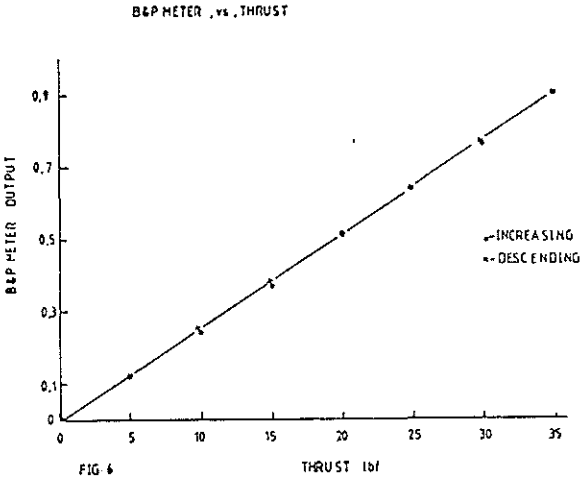

FIG 6

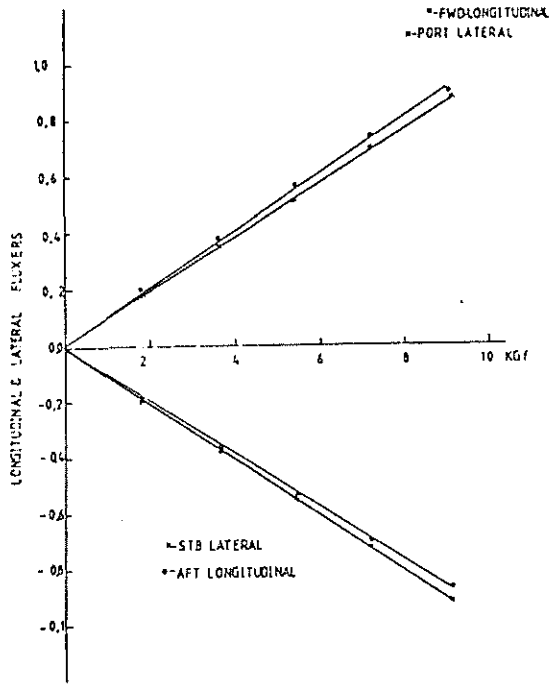

FIG-7 CALIBRATION LONGG LAT FORCES-

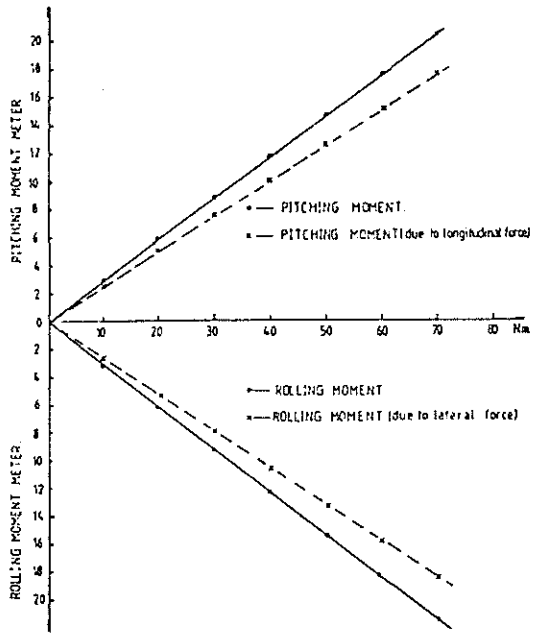

FIG 8 CALIBRATION CURVE FOR PITCHING & ROLLING MOMENTS

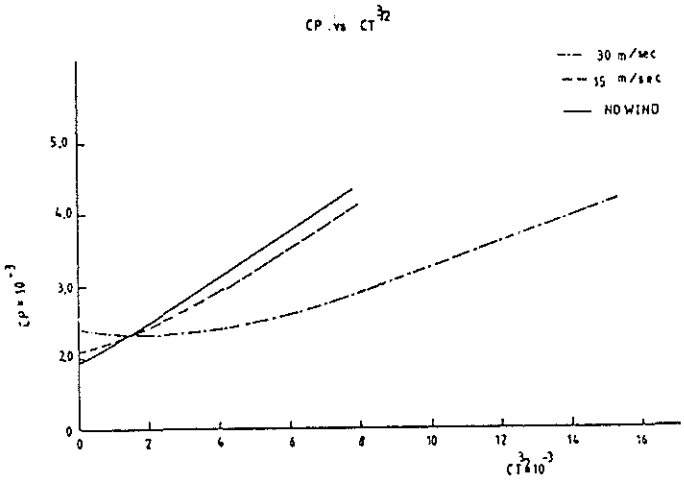

FIG 9

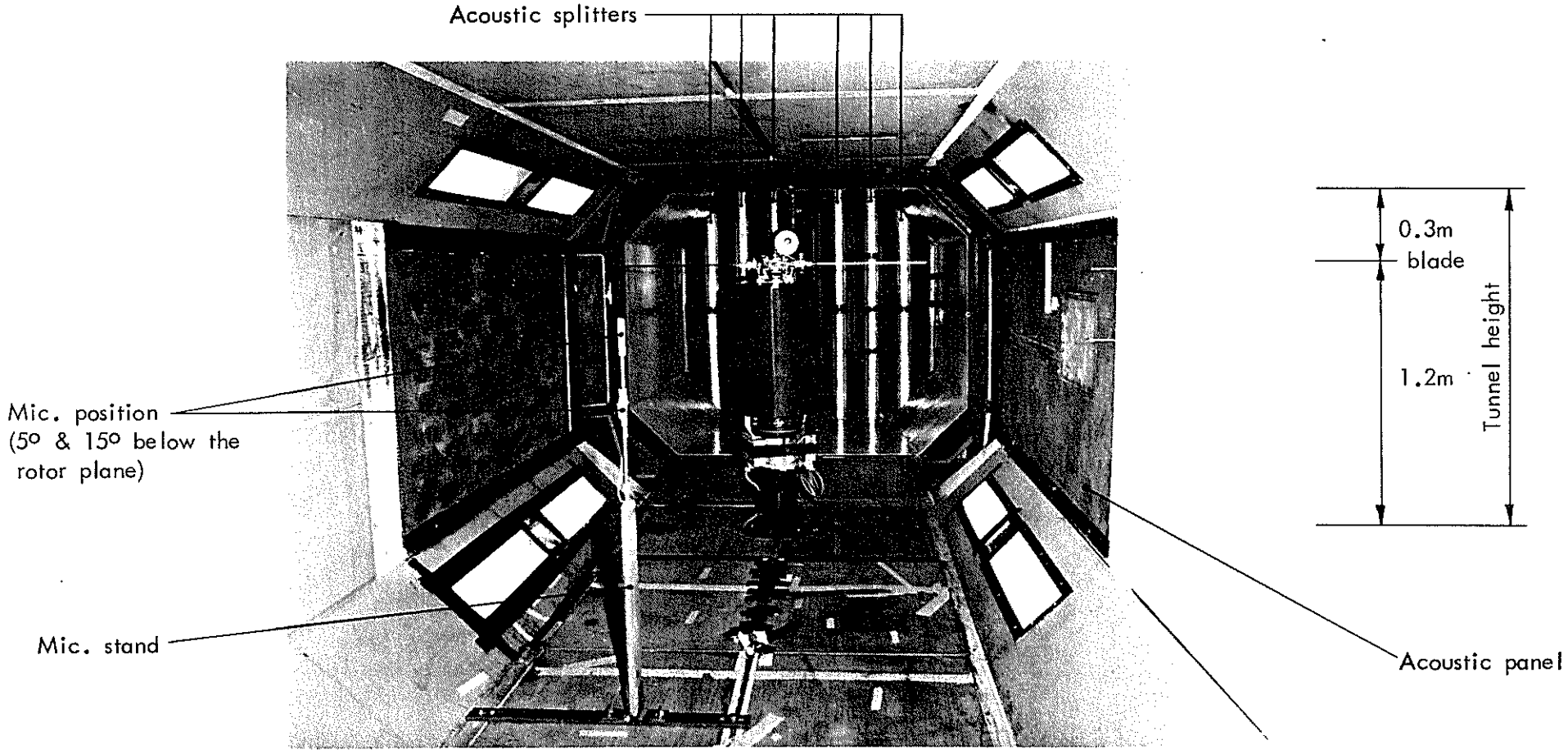

FIG.10 ROTOR MOUNTED IN THE ACOUSTIC TUNNEL

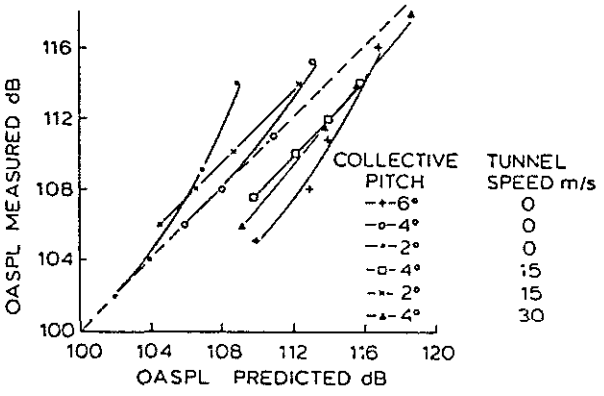

FIG.13 COMPARISON OF OASPL MEASURED & PREDICTED BY DAVIDSON AND HARGEST

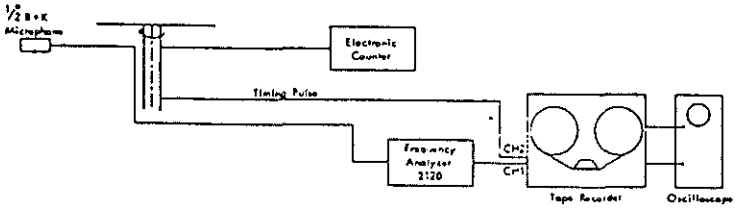

FIG.11 SCHEMATIC OF INSTRUMENTATION FOR ACQUISITION OF ACOUSTIC DATA

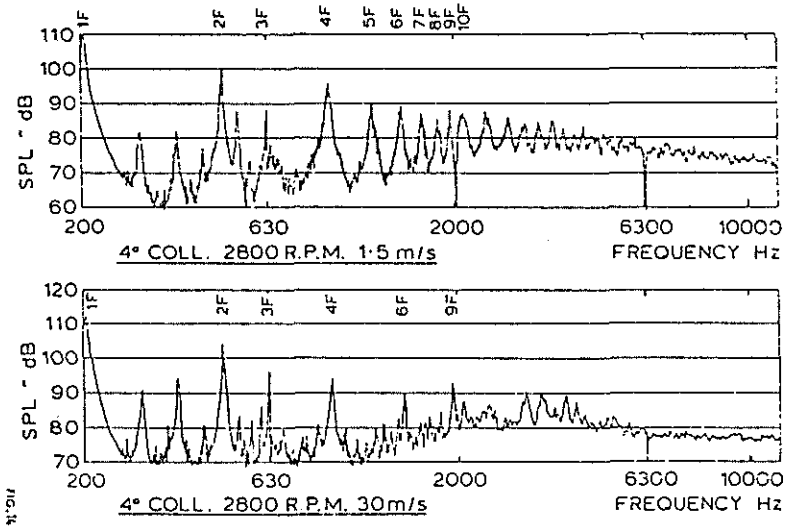

FIG.14 EFFECT OF FORWARD SPEED ON ROTOR AND NOISE SPECTRA

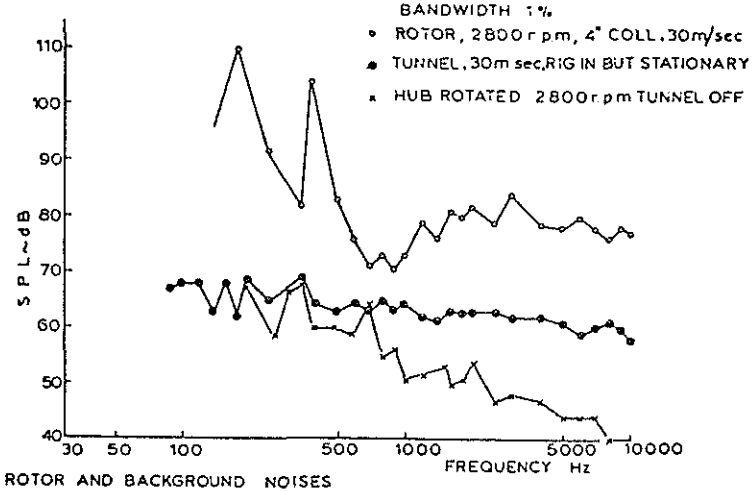

FIG.12 ROTOR AND BACKGROUND NOISES

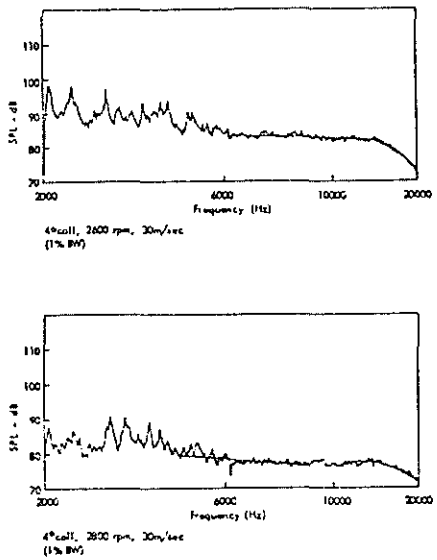

FIG. 17. HIGH FREQUENCY SPECTRUM

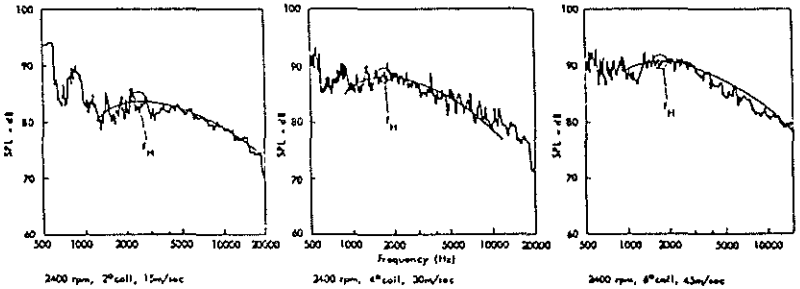

FIG. 15 ONE THIRD OCTAVE LOW FREQUENCY SPECTRUM

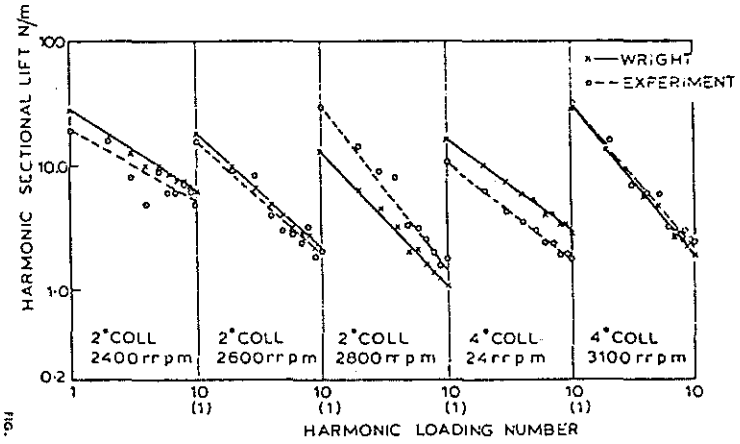

FIG. 18

ROTOR HARMONIC LOADING AT 0·85 SPAN TUNNEL SPEED 30 m/s

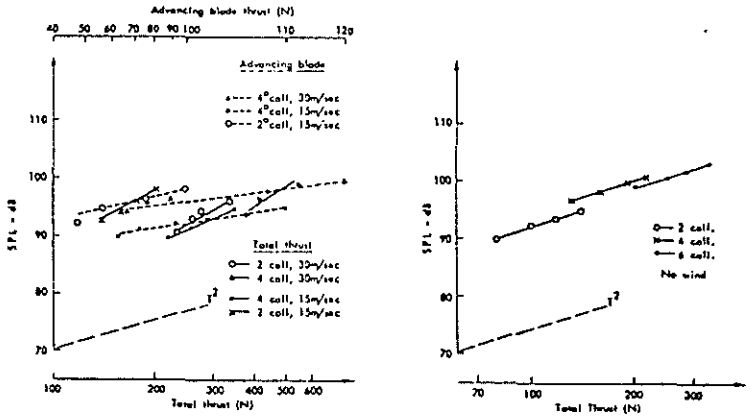

FIG. 16 LOW FREQUENCY BROAD BAND NOISE Vs. THRUST

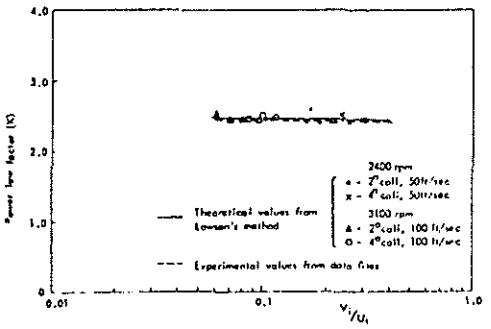

FIG.19 POWER LAW FACTOR (K) VS. SKEW ANGLE

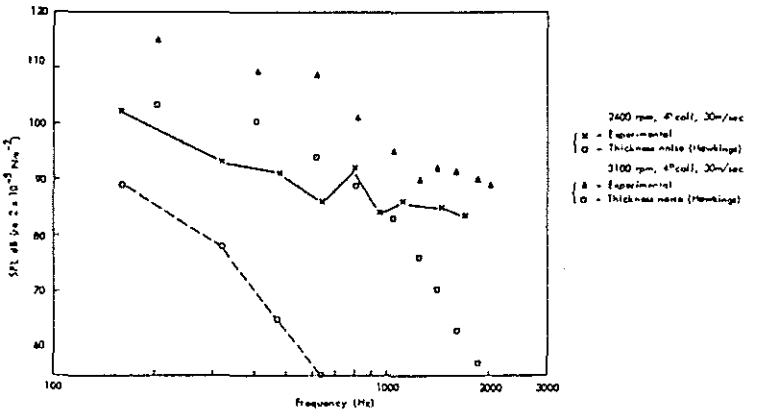

FIG.20 COMPARISON OF ROTOR ROTATIONAL NOISE WITH THICKNESS NOISE vs. FREQUENCY

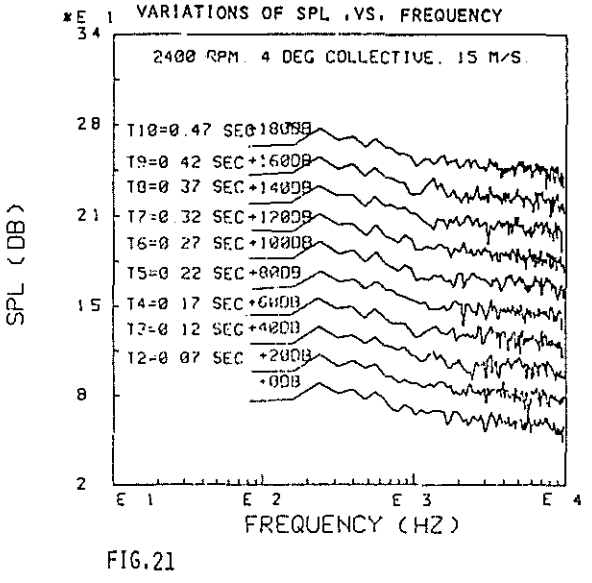

FIG.21

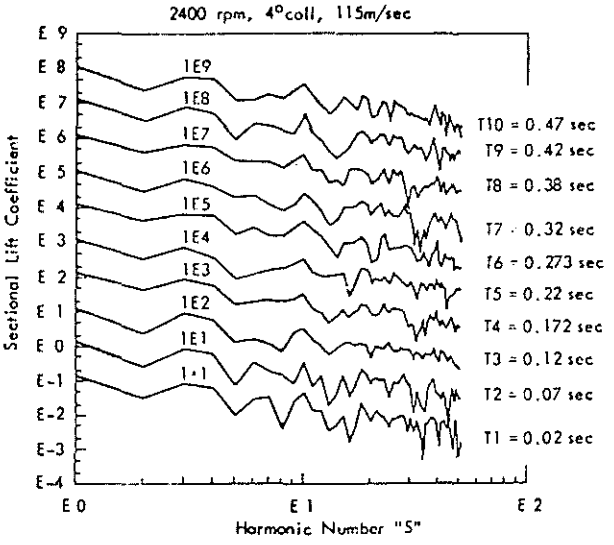

FIG.22 VARIATION OF LIFT COEFFICIENT (ie. TIME) VS. HARMONIC NO. "S"

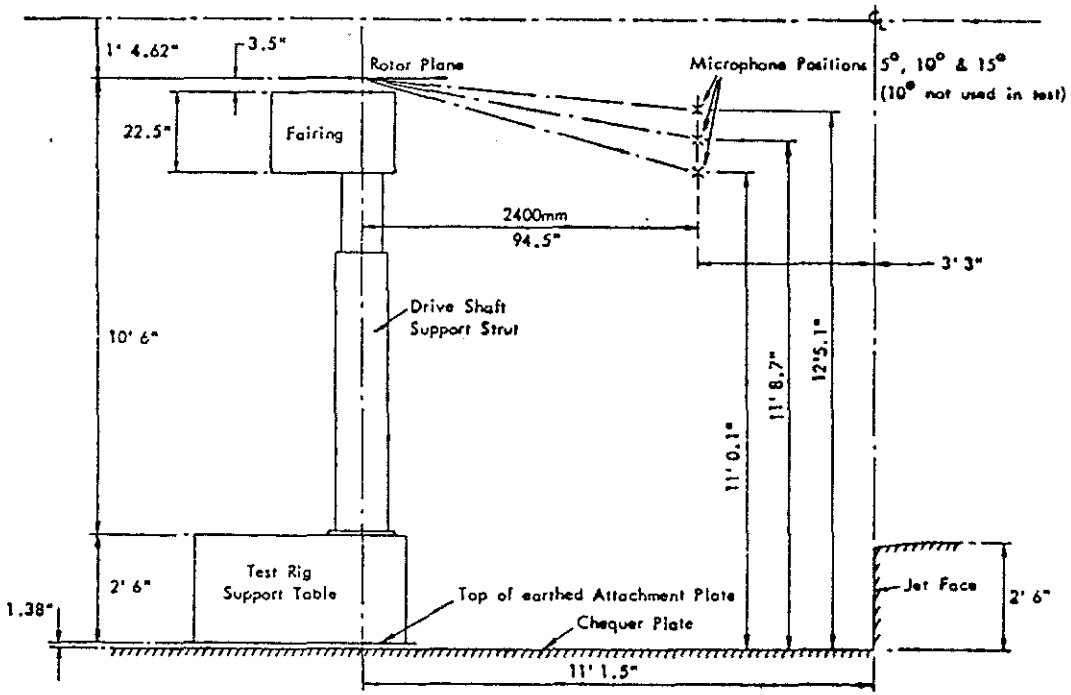

FIG.26 SOUTHAMPTON ROTOR RIG IN 24ft WIND-TUNNEL (not to scale)

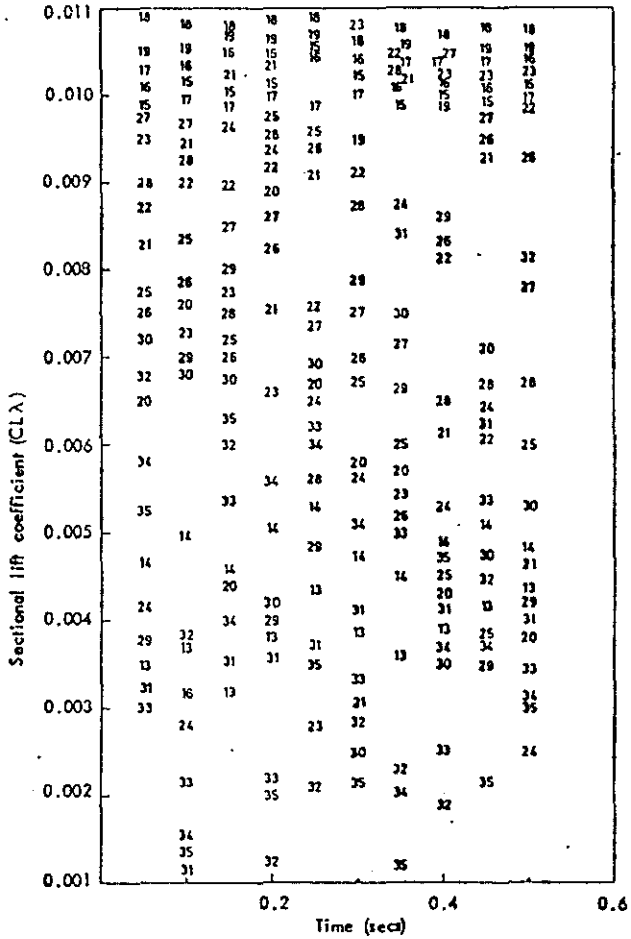

2400 rpm, 4° coll, 15m/sec

13 - 13th Harmonic
14 - 14th Harmonic
⋮
35 - 35th Harmonic

FIG. 27 VARIATION OF HARMONIC LIFT COEFFICIENTS CONTRIBUTED TO THE 6th NOISE HARMONIC LEVELS Vs TIME (sec).

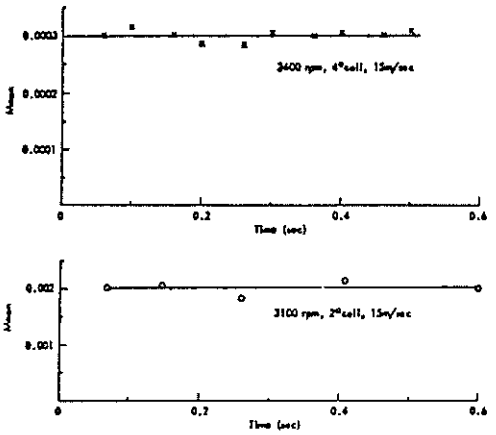

VARIATION IN MEAN OF NOISE SIGNAL Vs. TIME

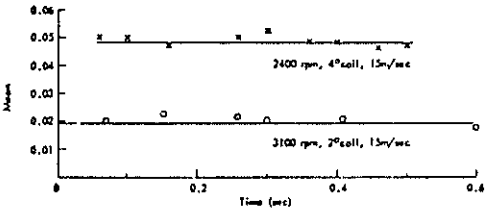

FIG.23 VARIATION IN MEAN OF HARMONIC LOADING Vs. TIME

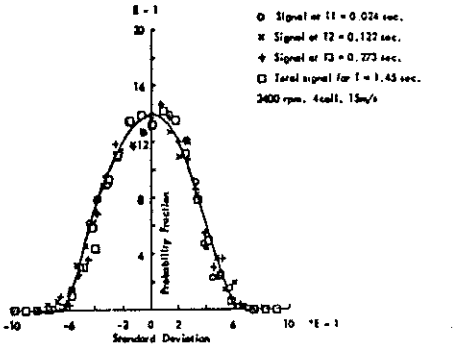

PROBABILITY DENSITY FUNCTION CURVE FOR ROTOR NOISE SIGNALS

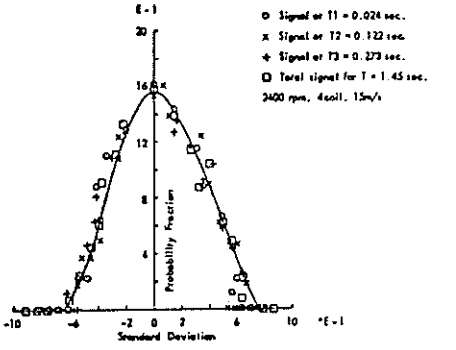

FIG. 24 PROBABILITY DENSITY FUNCTION CURVE FOR THE ROTOR LOADING SIGNALS.

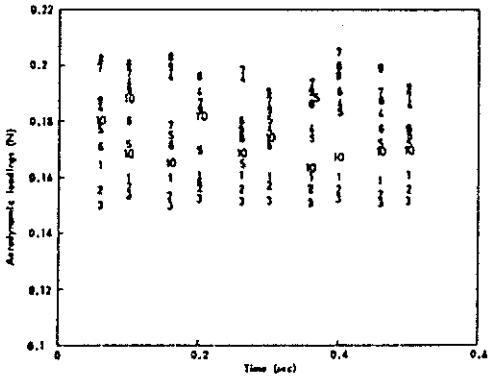

FIG.25 VARIATION OF HARMONIC LOADING Vs. TIME

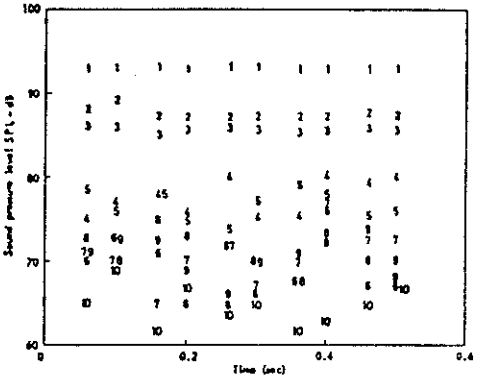

FIG.26 VARIATION IN HARMONIC S.P.L. Vs. TIME

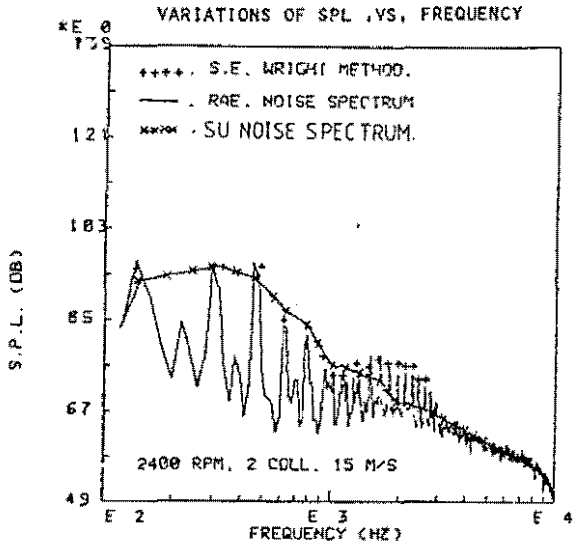

FIG.29

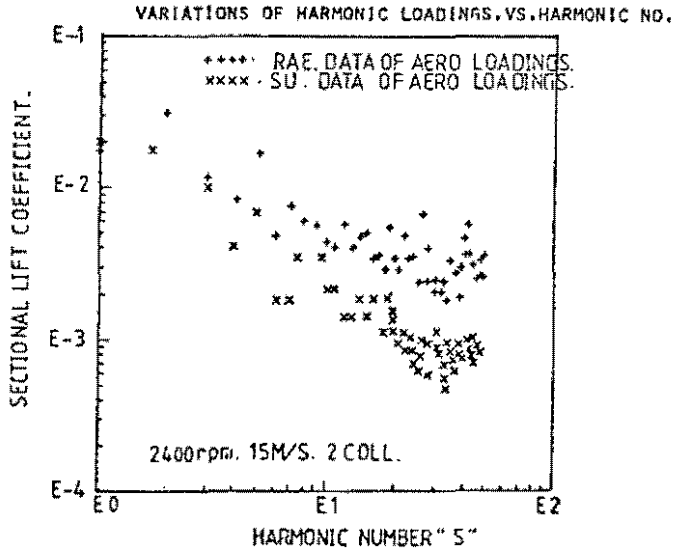

FIG.39

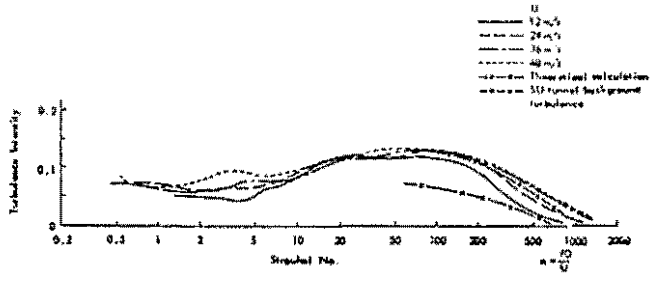

FIG. 31 SPECTRA OF TURBULENCE COMPONENTS IN RAE. 24 FT WIND - TUNNEL. MEASUREMENTS ON CENTRE-LINE.